

First principles electronic structure of spinel LiCr_2O_4 : A possible half-metal ?

Markus Lauer*

*Fachrichtung Theoretische Physik, Universität des Saarlandes,
Postfach 15 11 50, D-66041 Saarbrücken, Germany*

Roser Valenti†

*Institut für Theoretische Physik, Universität Frankfurt,
Robert-Mayer-Strasse 8, D-60054 Frankfurt, Germany*

H. C. Kandpal‡

Institut für Anorganische Chemie, Universität Mainz, Duesberg Weg 10-14, D-55099 Mainz, Germany

Ram Seshadri§

Materials Department, University of California, Santa Barbara, CA 93106 USA

We have employed first-principles electronic structure calculations to examine the hypothetical (but plausible) oxide spinel, LiCr_2O_4 with the $d^{2.5}$ electronic configuration. The cell (cubic) and internal (oxygen position) structural parameters have been obtained for this compound through structural relaxation in the first-principles framework. Within the one-electron band picture, we find that LiCr_2O_4 is magnetic, and a candidate half-metal. The electronic structure is substantially different from the closely related and well known rutile half-metal CrO_2 . In particular, we find a smaller conduction band width in the spinel compound, perhaps as a result of the distinct topology of the spinel crystal structure, and the reduced oxidation state. The magnetism and half-metallicity of LiCr_2O_4 has been mapped in the parameter space of its cubic crystal structure. Comparisons with superconducting LiTi_2O_4 ($d^{0.5}$), heavy-fermion LiV_2O_4 ($d^{1.5}$) and charge-ordering LiMn_2O_4 ($d^{3.5}$) suggest the effectiveness of a nearly-rigid band picture involving simple shifts of the position of E_F in these very different materials. Comparisons are also made with the electronic structure of ZnV_2O_4 (d^2), a correlated insulator that undergoes a structural and antiferromagnetic phase transition.

PACS numbers: 71.15.Nc, 71.20.-b, 75.50.-y

I. INTRODUCTION

The stoichiometric, self-doped oxide spinels LiM_2O_4 (with $M = \text{Ti}, \text{V}$ and Mn) can be said to constitute a periodic “hall of fame”. In all of them, Li is monovalent and the oxygen ion, negative and divalent; this means that the transition metal oxidation state is formally $3.5+$. The number of d electrons per transition metal atom would therefore be 0.5, 1.5, 2.5 or 3.5 when $M = \text{Ti}, \text{V}, \text{Cr}$ or Mn respectively. LiTi_2O_4 is a superconductor with a T_C of 12 K. When first prepared in 1973 [1] it was described as a high temperature superconductor. Along with $\text{BaBi}_{1-x}\text{Pb}_x\text{O}_3$ [2], it was amongst the only oxide superconductors with $T_C > 10$ K until the advent of the layered cuprates. It is also the *only* metallic oxide spinel known. Its neighbor, LiV_2O_4 is already on the verge of localization, and as a result, displays heavy-fermion behavior [3] — one of the few systems without f electrons that is known to do so — LiMn_2O_4 , one more member from this family, is not only a very important

cathode material in secondary Li-ion batteries [4], but also displays charge-ordering [5, 6], associated with half-integral charge that can order over two distinct sites. Indeed, the well-known Verweij transition in ferrite associated with the ordering of charge on the spinel lattice [7] can perhaps be best understood by examining LiMn_2O_4 . Near the charge-ordering temperature of this compound, a magnetic field can influence electrical transport and this translates to negative magnetoresistance [8].

Conspicuous in this list by its absence is the spinel LiCr_2O_4 . Attempts to prepare this compound are fraught with the difficulty of stabilizing Cr in a formal oxidation state that is somewhere between $3+$ and $4+$. Indeed ferromagnetic CrO_2 with the rutile structure is well known to require high oxygen partial pressures for its preparation. CrO_2 decomposes at ambient oxygen partial pressures when the temperature exceeds 473 K [9, 10]. Given that (i) the isostructural compounds neighboring LiCr_2O_4 are so interesting, and (ii) the structure and oxidation state of LiCr_2O_4 are reminiscent of CrO_2 , the prototypic oxide half-metal [10, 11], we thought the compound LiCr_2O_4 worthy of study.

In this work, we use spin-polarized first principles density functional calculations within two different schemes: Full potential linearized augmented plane-wave calculations [12, 13] that permit an optimization of the geome-

*Electronic address: mala@lusi.uni-sb.de

†Electronic address: valenti@lusi.uni-sb.de

‡Electronic address: kandpal@mail.uni-mainz.de

§Electronic address: seshadri@mrl.ucsb.edu

try of the cubic spinel compound (lattice parameter and internal structural parameter) and Linear Muffin Tin Orbital (LMTO) calculations [14] which are geared to the visualization of spin-resolved bonding. The electronic structure of LiCr_2O_4 is compared with that of rutile CrO_2 , LiM_2O_4 ($M = \text{Ti, V}$ and Mn), and ZnV_2O_4 . The parameter space of half-metallicity in LiCr_2O_4 is mapped out in terms of the two structural parameters.

II. CRYSTAL STRUCTURES AND COMPUTATIONAL METHODS

The cubic spinel crystal structure AB_2O_4 is completely described by two parameters, the cubic cell parameter a , and the internal oxygen positional parameter (x, x, x) where $x \sim 0.25$ [15]. The A atoms (Li) occupy tetrahedral sites created by a network of BO_6 octahedra where B is here a transition metal. The octahedra of oxygen around B are perfectly regular when $x = 0.25$. Deviations δ , $x = 0.25 + \delta$ indicate either a trigonal expansion ($\delta > 0$) or compression ($\delta < 0$), achieved by pushing two opposite triangular faces of the octahedron apart or together. The B atom sublattice (Cr in LiCr_2O_4) comprises a network of B_4 tetrahedra. Because the B atoms form tetrahedra, antiferromagnetic ordering is frustrated on the B site of the spinel [16] in a manner reminiscent of the residual entropy problem in the crystal structure of ice Ih [17]. Various views of the spinel crystal structure, and the structure of rutile CrO_2 are shown in Fig. 1.

Scalar-relativistic Kohn-Sham equations were solved taking all relativistic effects into account except for the spin-orbit coupling. We performed both full potential linearized augmented plane-wave (LAPW) calculations based on the WIEN97 and WIEN2K codes [12, 13] as well as Linear muffin-tin orbital (LMTO) calculations [14] within the atomic sphere approximation (ASA) where we used the STUTTGART TB-LMTO-ASA program [18]. The generalized gradient approximation (GGA) for the calculation of exchange correlation was considered following the Perdew-Burke-Ernzerhof [19] parameterization for the LAPW calculations and the Perdew-Wang prescription [20] for the LMTO calculation [21].

In our LAPW calculations we considered twenty inequivalent sampling k points and the modified tetrahedron method [22] for the Brillouin zone integration during the self-consistent iterations. In order to test the accuracy of the sampling, we also performed calculations with up to 120 and 195 irreducible k -points without observing significant qualitative changes in the results apart that some spikes in the density of states plots get rounded. We set the energy threshold between core and valence states at -6 Ryd [23]. For the number of plane waves, the criterion used was $\text{RMT} (\text{Muffin-Tin Radius}) \times k_{\text{max}}$ (for the plane waves) = 8. We considered various sets of muffin-tin radii to ensure well converged spin-polarized calculations.

In our LMTO calculations 256 irreducible k points

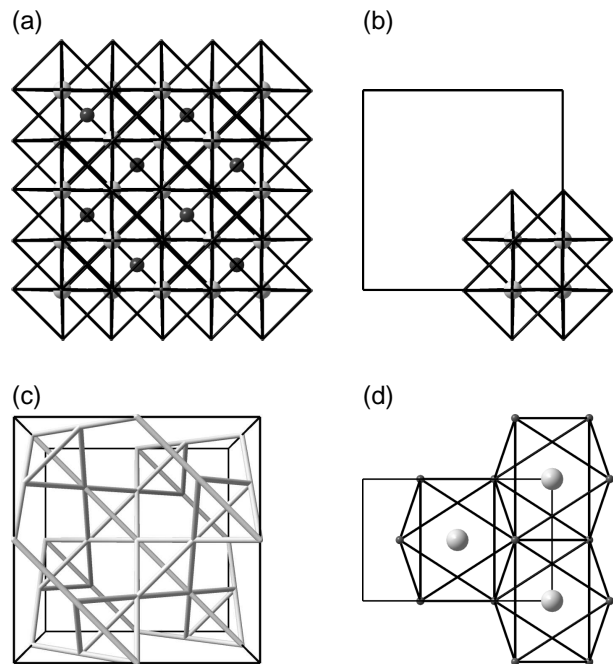


FIG. 1: (a) Spinel AB_2O_4 structure showing octahedral B atoms (grey spheres) at the centers of O_6 octahedra (depicted using sticks). The black spheres are the tetrahedrally coordinated A atoms. (b) Four BO_6 octahedra in the spinel structure showing the formation of B_4 tetrahedra as well as the nature of the edge-sharing of oxygen. (c) Network of corner-sharing B_4 tetrahedra in the spinel structure. (d) Portion of the crystal structure of rutile CrO_2 showing Cr atoms (grey spheres) in the middle of O_6 octahedra.

were used in the primitive wedge of the BZ. Space filling in the unit cell of LiCr_2O_4 was ensured through the use of two empty spheres with bases of s and p orbitals at $(0, 0, 0)$ and $(y, 1/8, 1/8)$ where the value of y is set automatically by the code according to the oxygen position. LMTO electronic structures were analyzed by calculating crystal orbital Hamiltonian populations (COHPs) [24] which are densities of states weighted by appropriate Hamiltonian matrix elements. COHPs are indicative of the strength and nature of a bonding (positive COHP) or antibonding (negative COHP) interaction. The signs we use here are the opposite of what is used in the original definition of Dronskowski and Blöchl [24]. LMTO-ASA calculations do not allow for structural relaxation while structural relaxation process is implemented in the LAPW package. We will present in what follows a comparison of the results obtained by both methods.

III. CRYSTAL AND ELECTRONIC STRUCTURE OF LiCr_2O_4

A. Structure optimization

Within the LAPW scheme we performed a structure optimization for LiCr_2O_4 where the cubic cell parameter a and the oxygen position x were varied till the optimal structure was obtained. In order to perform the optimization we considered two steps: (i) We first took several crystal structures with different lattice constants a and the same x . For each of them we performed an iteration procedure up to self-consistency and we compared the total energies. The energy minimum then defines the optimal a . For LiCr_2O_4 the energy minimum was reached at $a = 8.11(4)$ Å (see Fig. 2).

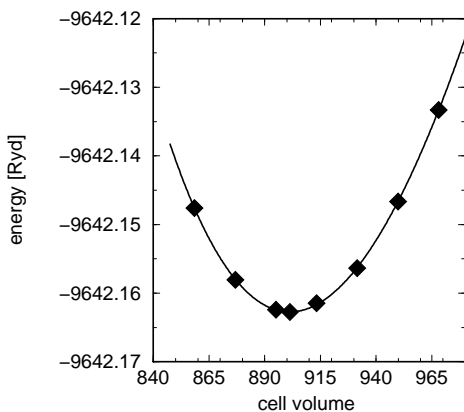


FIG. 2: LAPW energy versus primitive unit cell volume (in Bohr³) for the LiCr_2O_4 system. The squares are calculated LAPW data and the dashed curve is a fit to the Murnaghan equation of state [25]

(ii) In a second step we proceeded to optimize the oxygen positions by evaluating the atomic forces [26]. The equilibrium oxygen position was obtained using a damped Newton dynamics method according to the expression

$$R_m^{t+1} = R_m^t + \eta_m(R_m^t - R_m^{t-1}) + \delta_m F_m^t \quad (1)$$

where R_m^t and F_m^t are the coordinate and force for the atom m at time step t . δ_m determines the speed of motion and η_m changes from η_m to $1 - \eta_m$ if the force changes its direction from one step to the next. The optimal value we obtained for the oxygen position was $x = 0.253(5)$ which implies a small distortion from the perfect spinel structure. A further unit-cell optimization did not change the result significantly.

In the previous calculation scheme the unit-cell is first optimized and then the structure relaxed. Since the two operations do not necessarily commute, we considered also first a structural relaxation in a bigger unit cell fol-

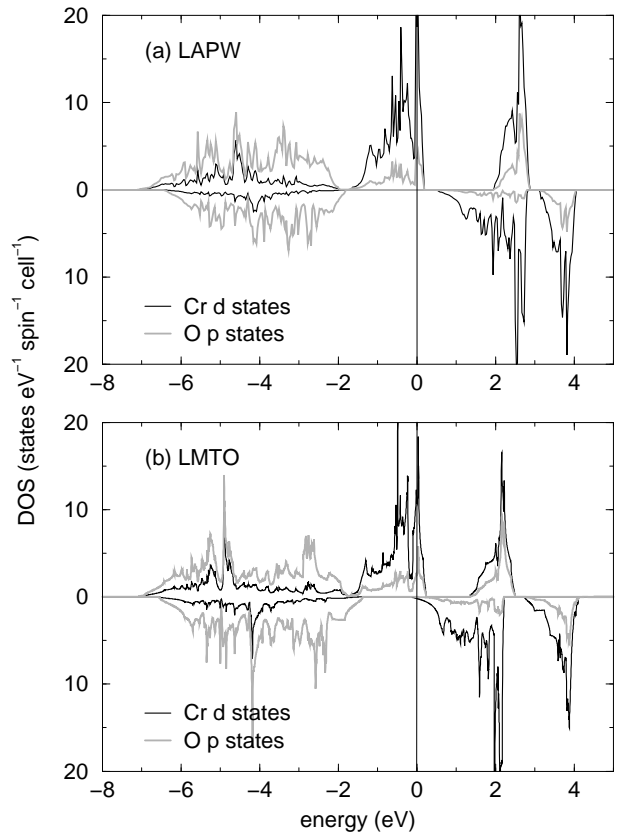


FIG. 3: (a) LAPW and (b) LMTO projected densities of states for LiCr_2O_4 . Black traces indicate Cr d states and grey traces indicate O p states. Spin up states are shown in the upper portions and spin down states in the lower portions in both panels. The origin on the energy axis in this and in the following plots is the E_F .

lowed by a lattice constant optimization. The two procedures do not yield exactly the same optimal value for a and x , but deviations from $a = 8.11(4)$ and $x = 0.253(5)$ are small and can be considered within the error bars.

We checked both in LAPW and LMTO that the ferromagnetic spin-polarized configuration is lower in energy than the non-spin-polarized case. We also considered within LAPW an antiferromagnetic spin arrangement of the Cr atoms in the spinel lattice which showed to be energetically unfavourable with respect to the ferromagnetic arrangement.

B. Density of states (DOS)

Figure 3 compares the partial density of chromium d states and oxygen p states from spin polarized (a) LAPW calculations and (b) LMTO calculations. In both plots, the Fermi energy is taken as the origin on the energy axis. The upper panel of each plot displays majority (up) spin states and the lower panel minority (down) spin states. Cr- d states are shown using black traces and

O- p state using grey traces. The optimized crystal structure obtained from the LAPW calculations was used as the input crystal structure for the (unrelaxed) LMTO calculations. We note immediately that in terms of gross features, the two computational methods yield quite similar results, in terms both of band positions and widths, as well as details in the structures of the projected densities of state. Differences in the two plots arise only as a result of slightly larger gaps between occupied and unoccupied states between the two computational schemes; the LAPW calculations indicate larger (by 0.5 eV) crystal field splitting as well as larger exchange splitting (by the same magnitude). This different energy shift can be understood in terms of the different nature of the two schemes and that for open structures -as the spinels are- the LMTO approach is not as accurate as the LAPW approach. We use here therefore the LAPW results as a reference for accuracy.

O p states are found to be largely centered around -4.5 eV and possess a width of about 5 eV. There are also Cr d states in this energy region, indicative of covalency. Near E_F we find majority Cr t_{2g} (\uparrow) and no minority spins in the LAPW DOS, i.e. the polarization is 100% what characterizes the system as half-metallic. In the LMTO DOS there is a residual spin density of minority Cr t_{2g} (\downarrow) spins at E_F . While strictly speaking the LMTO results predict an *approximate* half-metal behavior, the small overall differences between both LMTO and LAPW approaches justifies the use of the LMTO-ASA calculations in some of the subsequent discussion.

The $t_{2g}(\uparrow)$ states have a width of about 2 eV and are bimodal, with the two modes separated by a pseudo-gap. The E_F lies in the center of a peak in the DOS. The crystal field splitting between $t_{2g}(\uparrow)$ and $e_g(\uparrow)$ is of the order of 3 eV (taking the midpoints of the different manifolds) and the exchange splitting between $t_{2g}(\uparrow)$ and $t_{2g}(\downarrow)$ is of the order of 2 eV. These values are in the LMTO DOS -as discussed above- about 0.5 eV larger.

The two-peaked $t_{2g}(\uparrow)$ DOS is puzzling. One suspect is the trigonal distortion of the oxygen octahedron around the Cr atoms. In LiCr_2O_4 , the calculated oxygen position 0.253(5) suggests a very small distortion from perfect octahedral coordination. We have performed LMTO calculations using the ideal oxygen position $x = 0.250$ corresponding to perfect CrO_6 octahedra. The differences in the DOS (between the structures where $x = 0.25$ and $x = 0.253$) are negligible and the two-peaked structure of the $t_{2g}(\uparrow)$ DOS is retained, and E_F continues to fall in the second DOS peak even when O atoms are in the ideal position and the CrO_6 octahedra are undistorted.

Bimodal $t_{2g}(\uparrow)$ states, also observed in the electronic structure of spinel LiTi_2O_4 [27], could arise from the restricted B-O-B dispersion in the spinel structure; this network can be built up from B_4O_4 cubes that are interconnected through B atoms. The B-O-B bond angles are therefore 90° . This limits dispersion significantly. In fact, through the analysis of the COHP in LiCr_2O_4 in the next section we can identify that the upper lobe of the

DOS corresponds mainly to Cr-O interactions and less to Cr-Cr interactions.

The most important conclusion that we draw from the DOS of *ferromagnetic* LiCr_2O_4 is that states at and near E_F are strongly spin-polarized and the system is indeed a magnetic half-metal. However, the fact that E_F falls on a sharply peaked region of the DOS suggests (i) that the compound might be unstable/difficult to prepare and (ii) if it is prepared, might be subject to electronic instabilities associated with electron correlation, i.e. the opening of a Mott-Hubbard gap, or charge-ordering. We suggest that various different scenarios could stabilize the structure of LiCr_2O_4 , for instance the presence of a slightly distorted antiferromagnetic structure as it is the case in ZnV_2O_4 . Also if the system gets a little oxidized, by removing for instance some Li to form $\text{Li}_\delta\text{Cr}_2\text{O}_4$, where $\delta < 1$, it may be then possible to have E_F sitting in the pseudogap of the DOS, i.e. at the center of the bimodal DOS and therefore to have a stable structure. A third possibility, as mentioned above, is the explicit consideration of the electron correlation which may open a Mott-Hubbard gap at E_F and therefore settle stability.

C. Comparisons with CrO_2

It is important to compare the electronic structure of LiCr_2O_4 with the prototypic oxide half metal CrO_2 . Present understanding of this material has been reviewed recently [28]. This rutile compound Fig. 1(d) has d^2 Cr^{4+} surrounded octahedrally by O^{2-} . The octahedra form ribbons that share edges, and each Cr can therefore be said to bond with two others through the shared edge with a Cr-Cr distance of 2.92 Å [29]. A number of authors [30] have described the electronic structure of this material, including Korotin *et al.* [31] who performed LDA + U calculations and argue thereof that the one-electron description of a ferromagnetic band metal does not suffice and that $U = 3.0$ eV is required to explain the essential features of this compound. Mazin *et al.* [32] argued that when the local interaction is small compared to the bandwidth (W) $U/W \approx 0.5$ as in CrO_2 , it is disputable which method spin-polarized LDA or LDA+ U provides a better description of the system.

We have performed spin-polarized LDA calculations in the LMTO scheme on CrO_2 for two reasons. The first is that it provides us a consistent comparison with LiCr_2O_4 . The second is that spin-polarized bonding through the use of COHPs has not been presented before for this important compound. Figure 4 compares the Cr d and O p DOS of (a) LiCr_2O_4 and (b) CrO_2 . O p states of CrO_2 are found to be quite similar to what is seen for LiCr_2O_4 , spreading from around -7 eV to -2 eV. Once again, there is a strong admixture of Cr d states in this energy region. The region near the Fermi energy comprised largely of Cr d states. The crystal field splitting between $t_{2g}(\uparrow)$ and $e_g(\uparrow)$ is also similar in both compounds, as might be expected considering the similarity in charge and co-

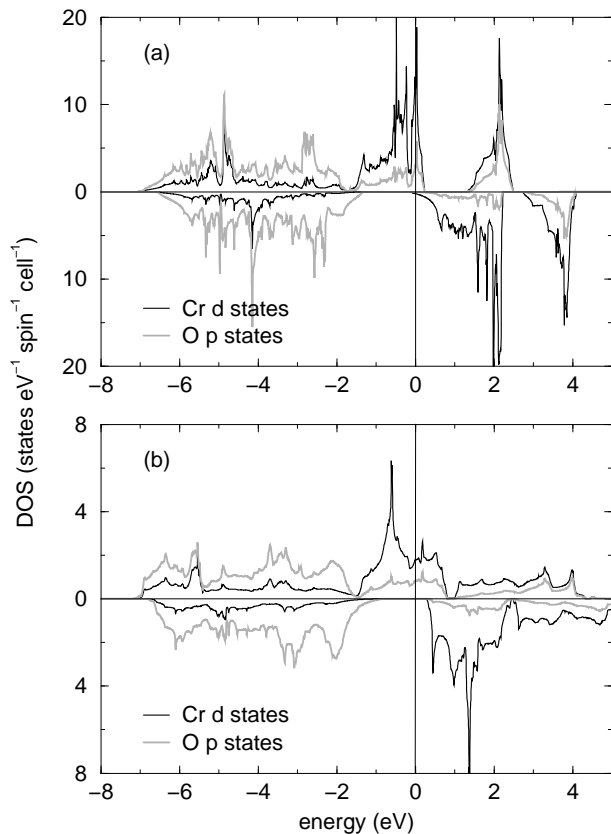


FIG. 4: LMTO projected densities of states for (a) LiCr_2O_4 and (b) CrO_2 . Black traces indicate Cr d states and grey traces indicate O p states.

ordination. What is significantly different is the larger $t_{2g}(\uparrow)$ bandwidth in CrO_2 , as a result of the different Cr-O topology in the rutile structure, that allows for easier metal-oxygen-metal hopping. Unlike what we see in LiCr_2O_4 , the E_F in CrO_2 does not lay on a peak but instead, lies on the edge of a pseudo-gap in the $t_{2g}(\uparrow)$ states. This gap arises due to a two-in, four-out Jahn-Teller distortion of the CrO_6 octahedra [29].

Crystal orbital Hamiltonian populations (COHPs) permit a better understanding of the precise nature of the different states that would determine the properties of LiCr_2O_4 . In Fig. 5, we plot (a) Cr-Cr COHPs and (a') Cr-O COHPs as a function of energy for LiCr_2O_4 , per primitive unit cell. This means Cr interacts with six O (at a distance of 2.00 Å) and to six other Cr (at a distance of 2.86 Å). The COHPs are spin resolved into interactions between orbitals with majority spin, and orbitals with minority spin. In the absence of spin-orbit coupling, majority states cannot bond with minority states. In the region of the DOS which was predominantly O- p (-7 eV to -2 eV) we find evidence for quite strong Cr-O covalency. At the E_F , we find a combination of majority antibonding Cr-Cr interactions and majority antibonding Cr-O interactions, being the Cr-O interaction predominant. There are no minority interactions near the E_F suggesting that

the bonding is highly spin-polarized. This is what makes this compound a putative half-metal.

Similar COHPs for CrO_2 [Fig. 5(b) and (b')] are depicted *per* unit cell. In CrO_2 , each Cr has 6 oxygen neighbors (4 at 1.90 Å and 2 at 1.91 Å), but only two Cr neighbors (at 2.92 Å). The shorter Cr-O distance in CrO_2 , compared with LiCr_2O_4 reflects the slightly higher oxidation state of Cr. The Cr-O COHP suggests strong Cr-O bonding in both spin directions in the region where O p states are found. Cr-Cr bonding is insignificant in this structure, as a result of the larger Cr-Cr distance than what is found in the spinel, as well as fewer neighbors. This means that Cr $t_{2g}(\uparrow)$ states at the E_F are largely non-bonding. As in LiCr_2O_4 , the Cr-O antibonding states at E_F are completely spin-polarized and correspond to interactions in the majority spin channel.

D. Comparisons with other LiM_2O_4 , $M = \text{Ti, V}$ and Mn , and with ZnV_2O_4

It is of interest to compare the DOS of the compounds LiM_2O_4 , $M = \text{Ti, V, Cr}$ and Mn . LiTi_2O_4 is a superconductor. LiV_2O_4 is a metal on the verge of a metal-insulator transition, with correspondingly, an unusually large effective carrier mass [3]. LiMn_2O_4 is a correlated antiferromagnetic insulator at low temperatures and displays a charge-ordering transition near the room temperature [5, 6, 8]. A number of recent papers describe the electronic structure of LiV_2O_4 [33]. For example, Singh *et al.* [34] have performed LAPW calculations on LiV_2O_4 . They find some evidence for a separation of the t_{2g} manifold into a_{1g} and e'_g states as a result of the trigonal distortion of the VO_6 octahedra, which is large in this compound. This results in the presence of both flat and disperse bands near the E_F , the flat bands presumably giving rise to the effective mass enhancement. Mishra and Ceder [35] have reported density functional calculations on LiMn_2O_4 , but with an emphasis on structural stability, rather than on magnetism.

Figure 6 compares the LMTO DOS of LiM_2O_4 , $M = \text{Ti, V, Cr, Mn}$. For the V, Cr and Mn compounds, we found that the ferromagnetic spin-polarized configuration was energetically more favourable than the non-spin-polarized configuration. For the Ti compound, the ferromagnetic solution lies in LAPW and LMTO higher in energy than the non-spin-polarized solution. In fact in LMTO we started for this system with a ferromagnetic spin-polarized configuration and in the self-consistency cycles it gets increasingly non-spin-polarized. The width of the O p states in all three compounds is similar. The separation between O p and metal d states is largest in the V compound and smallest in the Mn compound. This is in keeping with the expectation that for a given oxidation state and coordination, moving to the right amongst transition metals results in a stabilization of metal d states. Such stabilization is in fact the basis of the evolution of the band gap in correlated transition metal com-

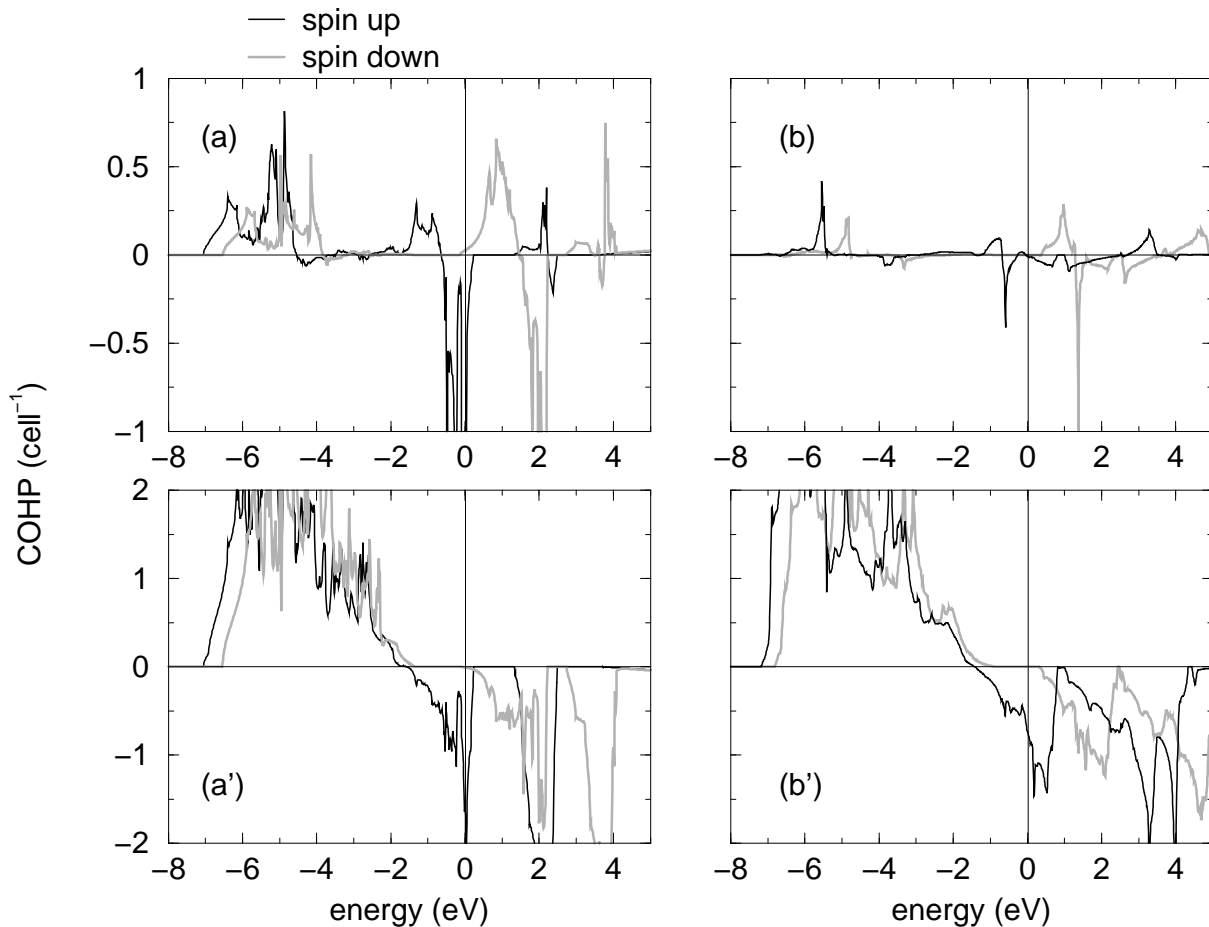


FIG. 5: Crystal orbital Hamiltonian populations (COHPs) in LiCr_2O_4 and CrO_2 per primitive unit cell. (a) Cr-Cr interactions in LiCr_2O_4 , (a') Cr-O interactions in LiCr_2O_4 , (b) Cr-Cr interactions in CrO_2 , (b') Cr-O interactions in CrO_2 . In each panel, the black trace corresponds to interactions in the spin up channel and the grey trace to interactions in the spin down channel.

pounds; from the Hubbard U type (arising from $d-d$ Coulomb correlation) for the early transition metals to charge-transfer Δ (arising from ligand to metal charge transfer) in the later transition metals [36, 37]. The width and gross features of metal t_{2g} states in these compounds display many similarities, and in fact, a simple rigid band picture of the DOS would perhaps suffice to describe the evolution on going from Ti through Mn. The t_{2g} manifold possesses a peaked region at the highest energy in all four compounds. In the Cr compound, this peaked region coincides with the Fermi energy. Interestingly, LiMn_2O_4 seems to be a low-spin system, with the electronic configuration $t_{2g}^3(\uparrow)$, $t_{2g}^{0.5}(\downarrow)$, which is distinctly different from the manganese oxides perovskites that display colossal magnetoresistance [38, 39]. In the perovskites, there is a gap between filled $t_{2g}^3(\uparrow)$ states and the partially filled states which are mostly $e_g(\uparrow)$ with some small admixture of O p and $t_{2g}(\downarrow)$.

The compound ZnV_2O_4 which is isostructural (spinel) and nearly isoelectronic (d electron count of 2 on the B site) with LiCr_2O_4 is known to be a Mott insulator [41]

ordering antiferromagnetically at 45 K [42], associated with a tetragonal distortion of the spinel unit cell. Recently Reehuis *et al.* [43] have performed a careful neutron diffraction study on this system. They find a structural transition from cubic $Fd\bar{3}m$ to tetragonal $I4_1/amd$ at 51(1) K which breaks the magnetic frustration of the spinel structure and allows an antiferromagnetic ground state to be obtained (with $T_N = 40(2)$ K). These authors have obtained precise nuclear and magnetic structures at 60 K (cubic, paramagnetic) and 1.8 K (tetragonal, antiferromagnetic). We have performed LAPW calculations on the cubic phase, and LMTO calculations on using both the cubic as well as the low temperature tetragonal structure [43]. The LAPW structure optimization gave a cell parameter of 8.348(3) Å to be compared with the 60 K experimental value of 8.4028(4) Å. The calculated internal x parameter of O was 0.259(4) Å (experiment = 0.2604(2)). The very close correspondence in this system provides confidence for the optimized LiCr_2O_4 structure. A magnetic moment of 1.84 μ_B per V was obtained from LMTO calculations on the cubic phase (1.85 μ_{rmB} from

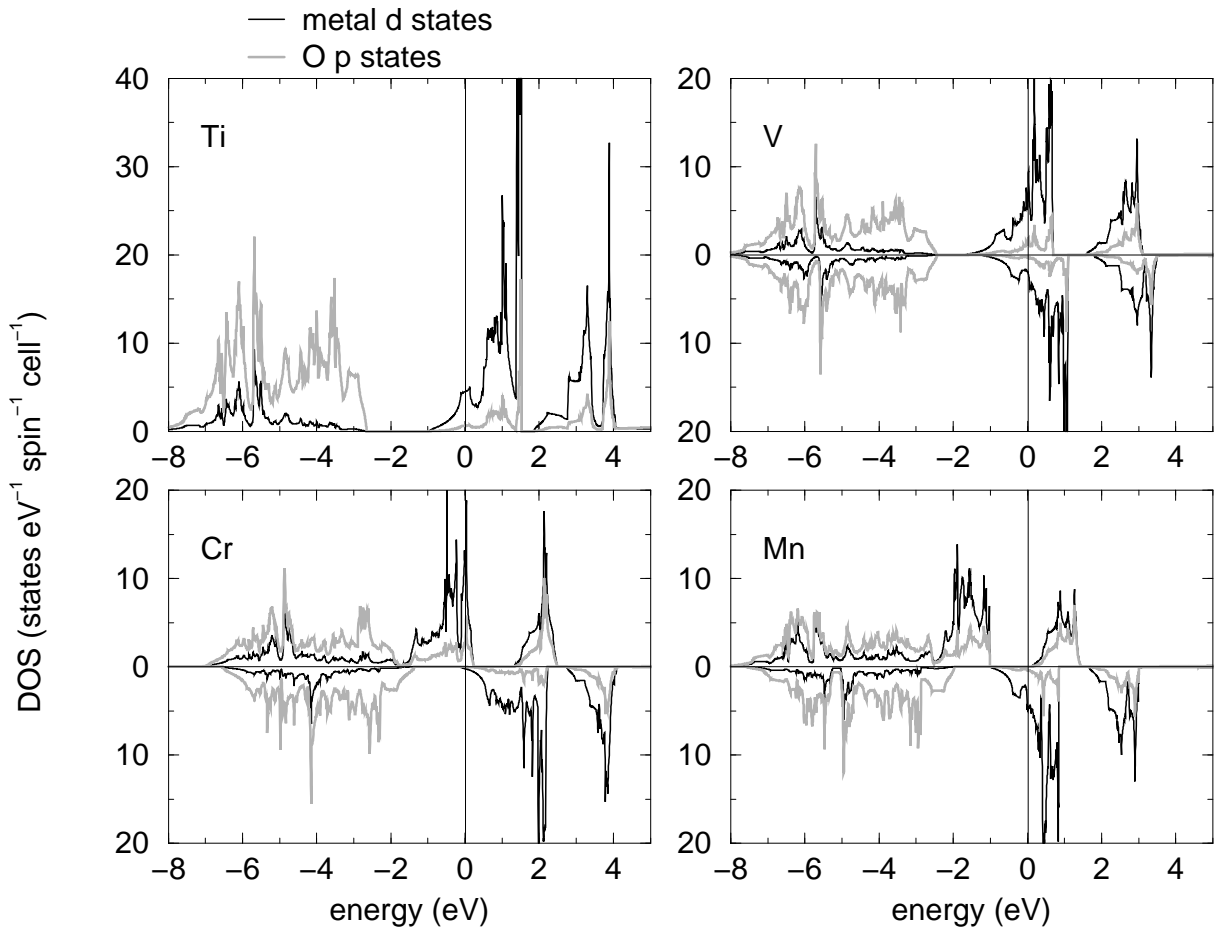


FIG. 6: LMTO (partial) density of states for LiM_2O_4 ($M = \text{Ti}, \text{V}, \text{Cr}, \text{Mn}$). Black traces indicate M d states and grey traces indicate O p states. Both LAPW and LMTO calculations yield spin-polarized ground states for the compounds with $M = \text{V}, \text{Cr}$ and Mn .

LAPW), indicating some reduction of the moment from the spin-only value of $2 \mu_B$. The DOS for V d states and O p states for spin-polarized cubic ZnV_2O_4 is displayed in Fig. 7(a). Key differences in the DOS of ZnV_2O_4 and LiCr_2O_4 include reduced metal-oxygen covalency corresponding to fewer V d states in the region of O p states. In addition, the Fermi energy no longer lies on a sharp DOS peak, despite similarities in the shapes of the $t_{2g}(\uparrow)$ manifolds. Cubic ZnV_2O_4 is a poorer half-metal when compared with LiCr_2O_4 as already manifest in the reduced magnetic moment. The d density of states of one of the V atoms in antiferromagnetic ZnV_2O_4 is displayed in Fig. 7(b). The LMTO calculations were performed on the experimental structure explicitly considering four independent V atoms forming a distorted tetrahedron with a short and a long V-V distance. The antiferromagnetic structure corresponds to spins on the tetrahedron being antiparallel when proximal (2.962 \AA) and parallel when far (2.963 \AA) in correspondence with experiment [43]. We observe that the DOS remains metallic, indicating that correlation must play an important role in this com-

pound, and that the one-electron description does not suffice. The changes in the DOS on going from the ferromagnetic cubic structure to the antiferromagnetic tetragonal structure include a slight narrowing of t_{2g} states and a reduction in the contribution from the DOS peak just below the E_F .

E. Magnetism of LiCr_2O_4

Spin polarized LMTO calculations suggested that the magnetic ground state for LiCr_2O_4 is more stable than the non-magnetic ground state obtained from a non-spin polarized calculation, by 0.4 eV per Cr atom. The converged magnetic moment on Cr was $2.49 \mu_B$ in calculations that made use of the non-local Perdew-Wang exchange correlation prescription. Since there are 2.5 d electrons per $\text{Cr}^{3.5+}$ in LiCr_2O_4 , the value of the magnetic moment corresponds to nearly 100% spin polarization (an extensive discussion was given in section II B.

Withing the usual von-Barth-Hedin LSDA [40], the

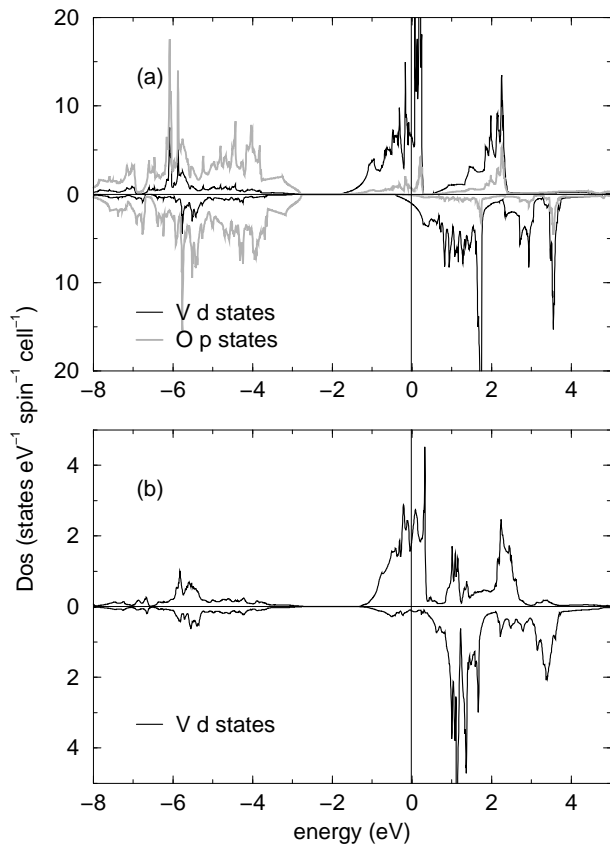


FIG. 7: (a) Partial DOS for cubic ZnV_2O_4 . Black traces indicate V d states and grey traces indicate O p states. (b) V d states for a single V atom in antiferromagnetic, tetragonal ZnV_2O_4 .

value was reduced to $2.42 \mu_B$ per Cr. We were interested in how changes in the crystal structure might affect the magnetism and half-metallicity in LiCr_2O_4 . To this end, we have mapped in Table 1, the magnetization M per Cr, as well as the extent of half-metallicity at E_F defined

$$P = \frac{N_{\uparrow}(E_F) - N_{\downarrow}(E_F)}{N_{\uparrow}(E_F) + N_{\downarrow}(E_F)} \times 100\%$$

as a function of the two structural parameters, the cubic

cell parameter a and the structural parameter δ which is a measure of the trigonal distortion of CrO_6 octahedra as described in section II. From Table 1, we see that larger unit cells favor a larger magnetic moment and larger P . This is due to the narrowing of bands as the separation between atoms becomes larger. Large values of δ seem to be contraindicated for magnetism and half-metallicity; the best half-metals correspond to nearly perfect CrO_6 octahedra. These results were confirmed by the structure optimization procedure of the LAPW calculations.

$a \setminus \delta$		-0.02	-0.01	0.00	0.01	0.015	0.02
8.00	M	0.00	0.00	2.46	2.47	2.46	2.43
	P	0	0	94	90	85	80
8.05	M	0.00	2.33	2.48	2.50	2.48	2.26
	P	0	65	96	91	87	86
8.10	M	0.00	2.42	2.49	2.50	2.49	2.27
	P	0	76	97	100	88	88
8.15	M	0.00	2.46	2.50	2.50	2.50	2.27
	P	0	88	99	100	93	91
8.20	M	0.62	2.49	2.50	2.50	2.50	2.50
	P	9	93	100	100	100	92
8.25	M	2.42	2.50	2.50	2.50	2.50	2.28
	P	83	100	100	100	100	94

TABLE I: Magnetic properties of LiCr_2O_4 (LMTO/GGA) as a function of the crystal structure. a is the cell parameter in \AA , δ is the deviation of the oxygen position from 0.25, M is the magnetization per Cr in μ_B , and P is the percentage spin polarization of conduction electrons.

Acknowledgments

This work was partially supported by the MRL program of the National Science Foundation under the Award No. DMR00-80034. RS would like to acknowledge a start-up grant from the Dean, College of Engineering, UCSB. RV thanks A. Krimmel for discussions and acknowledges financial support from the German Science Foundation.

-
- [1] D. C. Johnston, H. Prakash, W. H. Zachariasen and R. Viswanathan, *Mater. Res. Bull.* **8**, 777 (1973).
[2] A. W. Sleight, J. L. Gilson, and P. E. Bierstedt, *Solid State Commun.* **17**, 27 (1975).
[3] S. Kondo, D. C. Johnston, C. A. Swenson, F. Borsa, A. V. Mahajan, L. L. Miller, T. Gu, A. I. Goldman, M. B. Maple, D. A. Gajewski, E. J. Freeman, N. R. Dilley, R. P. Dickey, J. Merrin, K. Kijima, G. M. Luke, Y. J. Uemura, O. Chmaissem and J. D. Jorgensen, *Phys. Rev. Lett.* **78**, 3729 (1997).
[4] R. J. Gummow, A. deKock and M. M. Thackeray, *Solid State Ionics* **69**, 59, (1994); D. Guyomard and J. M. Tarascon, *Solid State Ionics* **69**, 222, (1994).
[5] J. Rodríguez-Carvajal, G. Rouse, C. Masquelier and M. Hervieu, *Phy. Rev. Lett.* **81**, 4660 (1998).
[6] R. Basu and R. Seshadri, *J. Mater. Chem.* **10**, 506 (2000).
[7] E. J. W. Verweij and P. W. Haaymann, *Physica (Utrecht)* **8**, 979 (1941).
[8] R. Basu, C. Felser, A. Maignan and R. Seshadri, *J. Mater. Chem.* **10**, 1921 (2000).

- [9] L. L. Chase, Phys. Rev. B. **10**, 2226 (1974); M. A. K. Dissanayake and L. L. Chase, Phys. Rev. B. **18**, 6872 (1978); K. Ramesha and J. Gopalakrishnan, J. Chem. Soc. Chem. Commun. 1173 (1999).
- [10] K. P. Kämper, W. Schmitt, G. Güntherodt, R. J. Gambino and R. Ruf, Phys. Rev. Lett. **59**, 2788, (1987).
- [11] R. J. Soulen Jr., J. M. Byers, M. S. Osofsky, B. Nadgorny, T. Ambrose S. F. Cheng, P. R. Broussard, C. T. Tanaka, J. Nowak, J. S. Moodera, A. Barry and J. M. D. Coey, Science **282**, 85, (1998).
- [12] P. Blaha, K. Schwarz and J. Luitz, WIEN97, *A Full Potential Linearized Augmented Plane Wave Package for Calculating Crystal Properties*, (K. Schwarz, Techn. Univ. Wien, Vienna 1999). ISBN 3-9501031-0-4. [Updated version of P. Blaha, K. Schwarz, P. Sorantin, and S. B. Trickey, Comp. Phys. Commun. **59**, 399 (1990)]. <http://www.wien2k.at>
- [13] G. K. H. Madsen, P. Blaha, K. Schwarz, E. Sjöstedt and L. Nördström, Phys. Rev. B **64**, 195134 (2001).
- [14] O. K. Andersen, Phys. Rev. B **12**, 3060 (1975); O. Jepsen and O. K. Andersen, Z. Phys. B **97**, 35 (1995).
- [15] Space group $Fd\bar{3}m$: A atoms at $(\frac{1}{8}, \frac{1}{8}, \frac{1}{8})$; B atoms at $(\frac{1}{2}, \frac{1}{2}, \frac{1}{2})$; O atoms at (x, x, x) . Alternate choices of the origin are possible in this space group.
- [16] P. W. Anderson, Phys. Rev. **102**, 1008 (1956).
- [17] L. Pauling, J. Am. Chem. Soc. **57**, 2680 (1935).
- [18] O. Jepsen and O. K. Andersen, The Stuttgart TB-LMTO-ASA Program version 47, MPI für Festkörperforschung, Stuttgart, Germany, 2000.
- [19] J. P. Perdew, K. Burke, and M. Ernzerhof, Phys. Rev. Lett. **77**, 3865 (1996).
- [20] J. P. Perdew and Y. Wang, Phys. Rev. B **33**, 8800 (1986); J. P. Perdew, J. A. Chevary, S. H. Vosko, K. A. Jackson, M. R. Pederson, D. J. Singh and C. Fiolhais, C. Phys. Rev. B **46**, 6671 (1992).
- [21] We also performed LAPW calculations using the Perdew-Wang prescription without observing for the DOS and bandstructures any appreciable differences to the Perdew-Burke-Ernzerhof results.
- [22] P. E. Blöchl, O. Jepsen, and O. K. Andersen, Phys. Rev. B **49**, 16223 (1994).
- [23] For LiV_2O_4 , LiMn_2O_4 and ZnV_2O_4 we took respectively as energy threshold -7, -7 and -10 Ryd.
- [24] R. Dronskowski and P. E. Blöchl, J. Phys. Chem. **97**, 8617 (1993); F. Boucher and R. Rousseau, Inorg. Chem. **37**, 2351 (1998).
- [25] F. D. Murnaghan, Proc. Nat. Acad. Sci. USA **30**, 244 (1944).
- [26] B. Kohler, S. Wilke, M. Scheffler, R. Kouba, and C. Ambrosch-Draxl, Comp. Phys. Commun. **94**, 31 (1996).
- [27] S. Satpathy and R. M. Martin, Phys. Rev. B **36**, 7269 (1987).
- [28] J. M. D. Coey and M. Venkatesan, J. Appl. Phys. **91**, 6671 (8345).
- [29] J. K. Burdett, G. J. Miller, J. W. Richardson and J. V. Smith, J. Am. Chem. Soc. **110**, 8064 (1988).
- [30] P. I. Sorantin and K. Schwarz, Inorg. Chem. **31**, 567 (1992); S. P. Lewis, P. B. Allen and T. Sasaki, Phys. Rev. B **55**, 10253 (1997).
- [31] M. A. Korotin, V. I. Anisimov, D. I. Khomskii and G. A. Sawatzky, Phys. Rev. Lett. **80**, 4305 (1998).
- [32] I. Mazin, D. J. Singh and C. Ambrosch-Draxl, Phys. Rev. B **59**, 411 (1999).
- [33] V. Eyert, K.-H. Höck, S. Horn, A. Loidl and P. S. Riseborough, Europhys. Lett. **46**, 762 (1999); V. I. Anisimov, M. A. Korotin, M. Zöfl, T. Pruschke, K. Le Hur and T. M. Rice, Phys. Rev. Lett. **83**, 364 (1999); J. Matsuno, A. Fujimori and L. F. Mattheiss, Phys. Rev. B. **60**, 1607 (1999).
- [34] D. J. Singh, P. Blaha, K. Schwarz and I. Mazin, Phys. Rev. B. **60**, 16357 (1999).
- [35] S. K. Mishra and G. Ceder, Phys. Rev. B **59**, 6120 (1999).
- [36] J. Zaanen, G. A. Sawatzky and J. W. Allen, Phys. Rev. Lett. **55**, 418 (1985).
- [37] T. Arima, Y. Tokura and J. B. Torrance, Phys. Rev. B **48**, 17006 (1993).
- [38] W. E. Pickett and D. J. Singh, Phys. Rev. B **53**, 1146 (1996); D. J. Singh and W. E. Pickett, Phys. Rev. B **57**, 88 (1998).
- [39] C. Felser, R. Seshadri, A. Leist and W. Tremel, J. Mater. Chem. **8**, 787 (1998).
- [40] U. von Barth and L. Hedin, J. Phys. C **5**, 1629 (1972).
- [41] A. Fujimori, K. Kawakami and N. Tsuda, Phys. Rev. B **38**, 7889 (1988).
- [42] Y. Ueda, N. Fujiwara and H. Yasuoka, J. Phys. Soc. Jpn. **66**, 778 (1997).
- [43] M. Reehuis, A. Krimmel, N. Büttgen, A. Loidl and A. Prokofiev, Eur. Phys. J. B. **35**, 311 (2003).